Applied Mathematics Letters 81 (2018) 35–43

Contents lists available at ScienceDirect

Applied Mathematics Letters

www.elsevier.com/locate/aml

An operator splitting strategy for fluid–structure interaction problems with thin elastic structures in an incompressible Newtonian flow☆

Aymen Laadhari

Institut für Bildverarbeitung, Department of Information Technology and Electrical Engineering, Swiss Federal Institute of Technology Zürich (Eidgenössische Technische Hochschule Zürich, ETH-Zentrum), CH-8092 Zürich, Switzerland

ARTICLE INFO

Article history:
Received 17 September 2017
Received in revised form 1 January 2018
Accepted 1 January 2018
Available online 8 January 2018

Keywords:
Newton method
Operator splitting
Navier–Stokes flow
Embedded interface
Finite element method

ABSTRACT

We present a computational framework based on the use of the Newton and level set methods to model fluid–structure interaction problems involving elastic membranes freely suspended in an incompressible Newtonian flow. The Mooney–Rivlin constitutive model is used to model the structure. We consider an extension to a more general case of the method described in Laadhari (2017) to model the elasticity of the membrane. We develop a predictor–corrector finite element method where an operator splitting scheme separates different physical phenomena. The method features an affordable computational burden with respect to the fully implicit methods. An exact Newton method is described to solve the problem, and the quadratic convergence is numerically achieved. Sample numerical examples are reported and illustrate the accuracy and robustness of the method.

1. Introduction

The individual and collective behaviors of red blood cells (RBCs) strongly influence the rheological properties of blood. The cytoskeleton (inner filamentous network of proteins) is responsible for the mechanical properties of RBCs and helps the cell to withstand hydrodynamic stresses without breaking. Understanding the RBC's mechanics provides a basis for predicting the hemorheology [1]. The modeling of RBCs entails the resolution of a difficult fluid–structure interaction (FSI) problem involving thin and highly deformable structures freely suspended in an incompressible fluid. This framework concerns the development of stable and efficient methodology to solve such a problem. At the numerical level, the large deformations of membranes in flow may induce several instability issues and immediately rule out a wide-set of numerical methods as candidates to describe such a dynamics, e.g. the Arbitrary Lagrangian Eulerian methods [2]. These instabilities are exacerbated for problems involving extremely slender and light

☆ This work was supported by ETH Zürich and the Swiss National Science Foundation award #320030-149567.
E-mail address: Aymen.Laadhari@math.ch.

https://doi.org/10.1016/j.aml.2018.01.001
0893-9659/

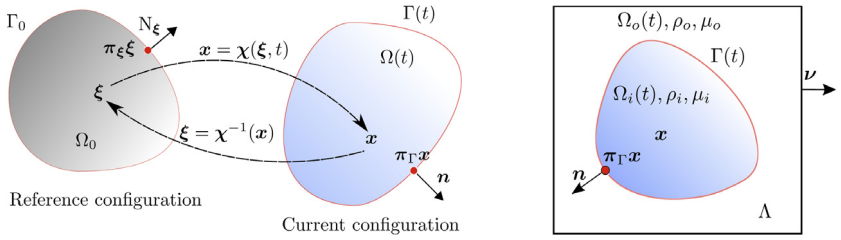

Fig. 1. Left: Schematic representation of a membrane in reference and current configurations. Right: Sketch for a membrane suspended in flow.

structures in incompressible flow. Embedded interface-type approaches are more appropriate to solve such a problem [2–5].

In this work we present a stable predictor–corrector numerical method based on the use of the Newton method and operator splitting algorithm to model elastic membranes in incompressible Newtonian flow.

2. Mathematical formulation

Let $T > 0$ and $d = 2, 3$ be the simulation period and space dimension, respectively. For any time $t \in (0, T)$, let $\Gamma(t)$ be an elastic membrane. The symmetric part of any tensor $\boldsymbol{T}$ is denoted by $\mathbf{sym}(\boldsymbol{T}) = \boldsymbol{T} + \boldsymbol{T}^T$. The tensorial product and the two times contracted product between tensors are denoted by the symbols "$\otimes$" and ":", respectively.

To model the deformations of extremely slender structures, the mathematical formulation is based on the theory of Gurtin and Murdoch for surface elasticity [6]. We subsequently write the problem in a purely Eulerian framework in the three-dimensional case and describe the numerical algorithm used to solve the resulting nonlinear problem.

2.1. Membrane elasticity model and governing equations

Consider the reference and current configurations as depicted in Fig. 1 (left). In the reference configuration ($t = 0$), the thin structure Γ_0 corresponds to the boundary of Ω_0. In the current configuration, the domain and membrane are represented by Ω and Γ, respectively. The forward characteristics $\boldsymbol{\chi} : (0, T) \times \Omega_0 \to \Omega$ map any particle's position $\boldsymbol{\xi} \in \Omega_0$ to $\boldsymbol{x} = \boldsymbol{\chi}(\boldsymbol{\xi}, t) \in \Omega$. Let $\boldsymbol{\nabla}_{\boldsymbol{\xi}}$ and $\boldsymbol{\nabla}$ be the gradient with respect to the material and spatial coordinates, respectively, while $\boldsymbol{\pi}_{\boldsymbol{\xi}} = \mathbf{I} - \mathbf{N}_{\boldsymbol{\xi}} \otimes \mathbf{N}_{\boldsymbol{\xi}}$ and $\boldsymbol{\pi}_\Gamma = \mathbf{I} - \mathbf{n} \otimes \mathbf{n}$ are the surface projectors onto Γ_0 and $\Gamma(t)$. Hence, $\boldsymbol{\nabla}_s = \boldsymbol{\pi}_\Gamma \boldsymbol{\nabla}$ and $\mathrm{div}_s = \mathrm{tr}(\boldsymbol{\nabla}_s)$ represent the surface gradient and divergence operators in the current configuration. A purely Eulerian representation of the mechanics shall write the constitutive law and elastic force with respect to the spatial coordinates. For instance, the deformation gradient tensor $\boldsymbol{F} \equiv \boldsymbol{\nabla}_{\boldsymbol{\xi}} \boldsymbol{\chi}$ writes $\boldsymbol{\nabla} \boldsymbol{\xi}^{-1}$ in an Eulerian framework. The membrane mechanics should depend on the surface deformation gradient $\boldsymbol{F}_s = \boldsymbol{\nabla}_{\boldsymbol{\xi}} \boldsymbol{x}\big|_\Gamma = \boldsymbol{\pi}_\Gamma \boldsymbol{F} \boldsymbol{\pi}_{\boldsymbol{\xi}}$, which lacks all out-of-plane strain components and is rank deficient [6]. Let λ_1 and λ_2 be the principal stretches: they represent the eigenvalues of the stretch tensor $\boldsymbol{\Lambda}$ in the local tangent plane to Γ. The left Cauchy–Green surface strain tensor is given by $\boldsymbol{B}_s = \boldsymbol{\Lambda}^2 = \boldsymbol{F}_s \boldsymbol{F}_s^T = \boldsymbol{\pi}_\Gamma \hat{\mathbf{B}}_\Gamma \boldsymbol{\pi}_\Gamma$ with $\hat{\mathbf{B}}_\Gamma = \boldsymbol{F} \boldsymbol{\pi}_{\boldsymbol{\xi}} \boldsymbol{F}^T$. Let $\boldsymbol{u}$ be the spatial velocity. To achieve an Eulerian description of the motion, the advection of $\boldsymbol{F}$ and $\boldsymbol{\pi}_{\boldsymbol{\xi}}$ leads to the following equation for the updated surface tensor $\hat{\mathbf{B}}_\Gamma$:

$$\partial_t \hat{\mathbf{B}}_\Gamma + \boldsymbol{u} \cdot \boldsymbol{\nabla} \hat{\mathbf{B}}_\Gamma = \mathbf{sym}\big(\boldsymbol{\nabla} \boldsymbol{u}\, \hat{\mathbf{B}}_\Gamma\big).$$

For a hyperelastic material, the stored energy function W shall be encoded in terms of the surface deformation tensor $\boldsymbol{F}_s$, that is, $\mathsf{W}\Big(\boldsymbol{F}_s\Big) = \mathsf{W}\Big(\boldsymbol{B}_s\Big) = \mathsf{W}\left(I_1^s, I_2^s\right)$ with I_1^s and I_2^s the surface strain invariants. They are

given by:

$$2I_1^s \equiv \ln\left(\lambda_1\lambda_2\right)^2 = \ln\left(\left(\mathrm{tr}\left(\boldsymbol{B}_s\right)\right)^2 - \mathrm{tr}\left(\boldsymbol{B}_s^2\right)\right) - \ln 2 \qquad \text{and} \qquad 2I_2^s \equiv \lambda_1^2+\lambda_2^2-2 = \mathrm{tr}\Big(\boldsymbol{B}_s\Big) - 2.$$

The local membrane area change between the reference and current configurations is given by $J_s \equiv \lambda_1\lambda_2 = \exp\left(I_1^s\right)$. To express the invariants in terms of $\hat{\mathbf{B}}_\Gamma$, we use $\mathrm{tr}\left(\boldsymbol{B}_s\right) = \boldsymbol{B}_s : \mathbf{I} = \hat{\mathbf{B}}_\Gamma : \boldsymbol{\pi}_\Gamma$ and $\mathrm{tr}\left(\boldsymbol{B}_s^2\right) = \hat{\mathbf{B}}_\Gamma\boldsymbol{\pi}_\Gamma$ $\hat{\mathbf{B}}_\Gamma : \boldsymbol{\pi}_\Gamma = \left(\hat{\mathbf{B}}_\Gamma\boldsymbol{\pi}_\Gamma\right)^2 : \mathbf{I}$. Accordingly, the strain invariants are given by:

$$2I_1^s = \ln\left(\left(\hat{\mathbf{B}}_\Gamma : \boldsymbol{\pi}_\Gamma\right)^2 - \left(\hat{\mathbf{B}}_\Gamma\boldsymbol{\pi}_\Gamma\right)^2 : \mathbf{I}\right) - \ln 2 \qquad \text{and} \qquad 2I_2^s = \boldsymbol{\pi}_\Gamma : \left(\hat{\mathbf{B}}_\Gamma - \mathbf{I}\right).$$

In the particular two-dimensional case, only one principal planar stretch exists, resulting in $J_s^2 = \hat{\mathbf{B}}_\Gamma : \boldsymbol{\pi}_\Gamma$. Hereafter, we consider a Mooney–Rivlin constitutive model. Let E_s be the membrane elastic modulus and $\zeta \in [0,1]$ be a nondimensional parameter. The surface strain energy and corresponding membrane Cauchy stress tensor read:

$$\begin{aligned}
\mathsf{W}\Big(\boldsymbol{F}_s\Big) = \mathsf{W}\Big(I_1^s, I_2^s\Big) &= \frac{E_s}{6}\zeta\left(2I_2^s\exp\left(-2I_1^s\right) + 2\exp\left(-2I_1^s\right) + \exp\left(2I_1^s\right) - 3\right) \\
&+ \frac{E_s}{6}(1-\zeta)\left(2I_2^s + \exp\left(-2I_1^s\right) - 1\right), \\
\boldsymbol{\sigma}_s\left(I_1^s, I_2^s\right) = \frac{1}{J_s}\frac{\partial \mathsf{W}}{\partial \boldsymbol{F}_s}\boldsymbol{F}_s^T &= \frac{1}{J_s}\sum_{i=1,2}\frac{\partial \mathsf{W}}{\partial I_i^s}\frac{\partial I_i^s}{\partial \boldsymbol{F}_s}\boldsymbol{F}_s^T \\
&= \frac{E_s}{3J_s}\left((1-\zeta)\Big(\boldsymbol{B}_s - \exp(-2I_1^s)\boldsymbol{\pi}_\Gamma\Big) + \frac{\zeta}{\exp(2I_1^s)}\Big(\boldsymbol{B}_s + \left(\exp(4I_1^s) - 2I_2^s - 2\right)\boldsymbol{\pi}_\Gamma\Big)\right).
\end{aligned}$$

Therefore, the membrane elastic force $\boldsymbol{\mathcal{F}}_\Gamma = \mathbf{div}_s\boldsymbol{\sigma}_s$ describes the discontinuity of the normal fluid stress tensor across the membrane Γ [6]. The choice $\zeta = 0$ results in the neo Hookean constitutive model for elastic membranes.

In what follows, $\Omega_i(t)$ and $\Omega_o(t) = \Lambda \setminus \Omega_i(t)$ represent the interior and exterior fluid domains of the elastic membrane $\Gamma(t)$, respectively, such that $\Gamma(t) \cap \partial\Lambda = \emptyset$, $\forall t \in (0,T)$, see Fig. 1 (right).

2.2. Statement of the nonlinear coupled problem

We adopt the level set method to implicitly follow the deformations of the membrane, which represents the iso-surface zero of a function φ such that $\Gamma(t) = \Big\{(t,\boldsymbol{x}) \in (0,T)\times\Lambda : \varphi(t,\boldsymbol{x}) = 0\Big\}$. The level set function is initialized as a signed distance and verifies the advection equation (2.1). A redistancing problem is regularly solved to keep the signed distance property [7]. Let ε be regularization parameter proportional to the mesh size h. The Heaviside function $\mathscr{H}$ and Dirac measure δ_Γ are regularized in a small band of width 2ε around Γ using the same expressions of the regularized $\mathscr{H}_\varepsilon(\varphi)$ and $\delta_\varepsilon(\varphi)$ provided in [8]. For any function $\psi(\cdot)$ defined on Γ, let $\tilde{\psi}(\cdot)$ be an extension to Λ such that it is constant in the normal direction to Γ. All surface integrals are approximated as follows:

$$\int_\Gamma \psi(\boldsymbol{x})\, d\boldsymbol{s} = \int_\Lambda \left|\nabla\varphi\right| \delta_\Gamma\, \tilde{\psi}(\boldsymbol{x})\, d\boldsymbol{x} \approx \int_\Lambda \left|\nabla\varphi\right| \delta_\varepsilon\left(\varphi\right)\, \tilde{\psi}(\boldsymbol{x})\, d\boldsymbol{x}.$$

The membrane is suspended in an incompressible Newtonian flow and we assume piecewise constant density $\rho_{i/o}$ and viscosity $\mu_{i/o}$. The corresponding regularized functions read $\rho_\varepsilon(\varphi) = \rho_i + (\rho_o - \rho_i)\mathscr{H}_\varepsilon(\varphi)$ and $\mu_\varepsilon(\varphi) = \mu_i + (\mu_o - \mu_i)\mathscr{H}_\varepsilon(\varphi)$. Let $\mathbf{D}(\boldsymbol{u}) = \mathbf{sym}(\nabla\boldsymbol{u})/2$ and $\boldsymbol{\sigma}_f = 2\mu(\varphi)\mathbf{D}(\boldsymbol{u}) - p\mathbf{I}$ be the strain and fluid Cauchy stress tensors, respectively. Equipped with initial and boundary conditions, the coupled problem

($\mathcal{P}$) reads: *find* $\Big(\varphi, \hat{\mathbf{B}}_\Gamma, \boldsymbol{u}, p\Big)$ *such that*

$$\partial_t \varphi + \boldsymbol{u}\cdot\boldsymbol{\nabla}\varphi = 0 \qquad \text{in } (0,T)\times\Omega, \tag{2.1}$$

$$\partial_t \hat{\mathbf{B}}_\Gamma + \boldsymbol{u}\cdot\boldsymbol{\nabla}\hat{\mathbf{B}}_\Gamma - \mathbf{sym}\Big(\boldsymbol{\nabla}\boldsymbol{u}\,\hat{\mathbf{B}}_\Gamma\Big) = \mathbf{0} \qquad \text{in } (0,T)\times\Omega, \tag{2.2}$$

$$\rho_\varepsilon(\varphi)\Big(\partial_t\boldsymbol{u} + \boldsymbol{u}\cdot\boldsymbol{\nabla}\boldsymbol{u}\Big) - \mathbf{div}\Big(2\mu_\varepsilon(\varphi)\mathbf{D}(\boldsymbol{u})\Big) + \boldsymbol{\nabla}p = \mathbf{0} \qquad \text{in } (0,T)\times\Omega, \tag{2.3}$$

$$\operatorname{div}\boldsymbol{u} = 0 \qquad \text{in } (0,T)\times\Omega, \tag{2.4}$$

$$\Big[\boldsymbol{u}\Big]_-^+ = \mathbf{0} \qquad \text{and} \qquad [\boldsymbol{\sigma}_f\mathbf{n}]_-^+ = -\mathbf{div}_s\boldsymbol{\sigma}_s \qquad \text{on } (0,T)\times\Gamma. \tag{2.5}$$

3. Finite element approximation and solution method

3.1. Time discretization: an operator splitting scheme

Following [9], an order one operator splitting scheme allows the advection and diffusion phenomena to be decoupled. Let us divide $[0,T]$ into N subintervals $\big[t_n, t_{n+1}\big]$ with $n = 0,\dots,N-1$ of constant time step Δt. For $n > 0$, the unknowns $\boldsymbol{u}_n$, p_n, $\hat{\boldsymbol{B}}_{\Gamma,n}$ and φ_n approximate $\boldsymbol{u}$, p, $\hat{\mathbf{B}}_\Gamma$ and φ at t_n, respectively. We introduce the functional spaces:

$$\mathbb{V}(\boldsymbol{u}_b) = \Big\{\boldsymbol{v}\in\big(H^1(\Lambda)\big)^d : \boldsymbol{v} = \boldsymbol{u}_b \text{ on } \partial\Lambda\Big\},\quad \mathbb{Q} = L^2_0(\Lambda),\quad \mathbb{W} = \Big\{\boldsymbol{\tau}\in\big(L^2(\Lambda)\big)^{d\times d} : \boldsymbol{\tau} = \boldsymbol{\tau}^T\Big\} \text{ and}$$
$$\mathbb{X} = W^{1,\infty}(\Lambda)\cap H^1(\Lambda).$$

Given the approximations of φ, $\boldsymbol{u}$ and $\hat{\mathbf{B}}_\Gamma$ at times t_{n-1} and t_{n-2}, the prediction step consists in solving in the interval $\big[t_{n-1}, t_n\big]$ the advection problems:

$$\partial_t\varphi + \boldsymbol{u}\cdot\boldsymbol{\nabla}\varphi = 0, \qquad \partial_t\hat{\mathbf{B}}_\Gamma + \boldsymbol{u}\cdot\boldsymbol{\nabla}\hat{\mathbf{B}}_\Gamma = \mathbf{0} \qquad \text{and} \qquad \partial_t\boldsymbol{u} + \boldsymbol{u}\cdot\boldsymbol{\nabla}\boldsymbol{u} = \mathbf{0}$$

using the method of characteristics. That yields the new level set function φ_n, the predicted velocity $\boldsymbol{u}_{n-1/2}$ and the predicted stress $\hat{\boldsymbol{B}}_{\Gamma,n-1/2}$. The scheme is bootstrapped by $\boldsymbol{u}_{-1} = \boldsymbol{u}_0$ where $\boldsymbol{u}_{-1}$ only stands for a suitable notation (likewise for $\hat{\mathbf{B}}_\Gamma$ and φ). Let $\tilde{\boldsymbol{u}} = 2\boldsymbol{u}_n - \boldsymbol{u}_{n-1}$ be the second order extrapolation of $\boldsymbol{u}$. The first and second-order characteristics are given by $X_n^{(1)}(\boldsymbol{x}) = \boldsymbol{x} - \Delta t\,\tilde{\boldsymbol{u}}(\boldsymbol{x})$ and $X_n^{(2)}(\boldsymbol{x}) = \boldsymbol{x} - 2\Delta t\,\tilde{\boldsymbol{u}}(\boldsymbol{x})$. The new membrane position is computed as follows:

$$\int_\Lambda 3\varphi_n\psi = \int_\Lambda 4\varphi_{n-1}\circ X_{n-1}^{(1)}\,\psi - \varphi_{n-2}\circ X_{n-1}^{(2)}\,\psi, \qquad \forall\psi\in\mathbb{X}.$$

Analogously, we compute $\boldsymbol{u}_{n-1/2}$ and $\hat{\boldsymbol{B}}_{\Gamma,n-1/2}$. Thereafter, the correction step consists in solving the problem ($\mathcal{P}$) without convection [9]. We employ the shorthand notation $\boldsymbol{\pi}_{\Gamma,n} = \mathbf{I} - \boldsymbol{\nabla}\varphi_n\otimes\boldsymbol{\nabla}\varphi_n/|\boldsymbol{\nabla}\varphi_n|^2$ to denote the discretized surface projector at t_n evaluated using the new level set function. Let $\boldsymbol{w}$ be a generic test function corresponding to $\boldsymbol{u}$.

To write the variational formulation, we use the identity $\boldsymbol{\sigma}_s\,\mathbf{n} = \mathbf{0}$ which leads to the following transformation:

$$\int_\Gamma \mathbf{div}_s\boldsymbol{\sigma}_s\cdot\boldsymbol{w} = -\int_\Gamma \boldsymbol{\sigma}_s : \boldsymbol{\nabla}_s\boldsymbol{w} = -\frac{E_s}{3}\int_\Gamma\left(\frac{\zeta}{J_s^3} + \frac{1-\zeta}{J_s}\right)\hat{\mathbf{B}}_\Gamma : \Big(\boldsymbol{\pi}_\Gamma\,\boldsymbol{\nabla}\boldsymbol{w}\,\boldsymbol{\pi}_\Gamma\Big)$$
$$+\left(\frac{\zeta}{J_s^3}\Big(J_s^4 - 2I_2^s - 2\Big) - \frac{1-\zeta}{J_s^3}\right)\operatorname{div}_s\boldsymbol{w}.$$

Equipped with predicted initial conditions $\boldsymbol{u}_{n-2} \leftarrow \boldsymbol{u}_{n-1}$, $\boldsymbol{u}_{n-1} \leftarrow \boldsymbol{u}_{n-1/2}$, $\hat{\boldsymbol{B}}_{\Gamma,n-2} \leftarrow \hat{\boldsymbol{B}}_{\Gamma,n-1}$ and $\hat{\boldsymbol{B}}_{\Gamma,n-1} \leftarrow \hat{\boldsymbol{B}}_{\Gamma,n-1/2}$, the corrected velocity $\boldsymbol{u}_n \in \mathbb{V}(\boldsymbol{u}_b)$, corrected stress $\hat{\boldsymbol{B}}_{\Gamma,n} \in \mathbb{W}$ and pressure $p_n \in \mathbb{Q}$ at t_n are computed by solving:

$$\int_\Lambda \frac{3\hat{\boldsymbol{B}}_{\Gamma,n} - 4\hat{\boldsymbol{B}}_{\Gamma,n-1} + \hat{\boldsymbol{B}}_{\Gamma,n-2}}{2\Delta t} : \boldsymbol{\tau} - \int_\Lambda \mathbf{sym}\left(\boldsymbol{\nabla u}_n \hat{\boldsymbol{B}}_{\Gamma,n}\right) : \boldsymbol{\tau} = 0, \qquad \forall \boldsymbol{\tau} \in \mathbb{W} \tag{3.1a}$$

$$\begin{aligned}
&\int_\Lambda \rho_\varepsilon(\varphi_n) \frac{3\boldsymbol{u}_n - 4\boldsymbol{u}_{n-1} + \boldsymbol{u}_{n-2}}{2\Delta t} \cdot \boldsymbol{v} - \int_\Lambda p_n \mathrm{div}\, \boldsymbol{v} \\
&\quad + \frac{E_s}{3} \int_\Lambda |\boldsymbol{\nabla}\varphi_n| \, \delta_\varepsilon(\varphi_n) \left(\frac{\zeta}{(J_{s,n})^3} + \frac{1-\zeta}{J_{s,n}}\right) \hat{\boldsymbol{B}}_{\Gamma,n} : \left(\boldsymbol{\pi}_{\Gamma,n} \boldsymbol{\nabla v} \boldsymbol{\pi}_{\Gamma,n}\right) \\
&\quad + \int_\Lambda 2\mu_\varepsilon(\varphi_n) \, \mathbf{D}(\boldsymbol{u}_n) : \mathbf{D}(\boldsymbol{v}) \\
&\quad + \frac{E_s}{3} \int_\Lambda |\boldsymbol{\nabla}\varphi_n| \, \delta_\varepsilon(\varphi_n) \left(\zeta J_{s,n} - 2\zeta \frac{I^s_{2,n}}{(J_{s,n})^3} - \frac{1+\zeta}{(J_{s,n})^3}\right) \boldsymbol{\pi}_{\Gamma,n} : \boldsymbol{\nabla v} = 0, \qquad \forall \boldsymbol{v} \in \mathbb{V}(0)
\end{aligned} \tag{3.1b}$$

$$\int_\Lambda q \, \mathrm{div}\, \boldsymbol{u}_n = 0, \qquad \forall q \in \mathbb{Q}. \tag{3.1c}$$

The particular energy $\mathsf{W}(\boldsymbol{F}_s) = \gamma J_s + c$, where the surface tension coefficient γ and c are constants, leads to a predictor–corrector strategy to solve the capillary problem [8]. That results in the following expressions of the stress tensor $\boldsymbol{\sigma}_s = \gamma \boldsymbol{\pi}_\Gamma$ and the capillary force $\boldsymbol{\mathcal{F}}_\Gamma = -\gamma H \mathbf{n}$.

3.2. Exact tangent problem and Newton–Raphson method

Let $\mathscr{R}(\boldsymbol{\chi})$ be the global residual corresponding to (3.1a)–(3.1b)–(3.1c) with $\boldsymbol{\chi} \equiv \left(\boldsymbol{u}, p, \hat{\boldsymbol{B}}_\Gamma\right)$ and $\langle ., . \rangle$ stand for the duality product. The Gâteaux derivative of $\mathscr{R}$ along the direction $\delta\boldsymbol{\chi}$ at $\boldsymbol{\chi}$ is denoted by $D\mathscr{R}(\boldsymbol{\chi})[\delta\boldsymbol{\chi}]$. We solve the nonlinear problem $\mathscr{R}(\boldsymbol{\chi}) = \mathbf{0}$ using the Newton method [10]. Given the solutions at t_n, we iteratively compute the increment $\delta\boldsymbol{\chi}_n^k$ until reaching a stopping criterion based on the residual computation. We set the Newton tolerance to $\epsilon_{tot} = 10^{-8}$. For any sub-iteration $k \geqslant 0$, the solution explicitly expresses as $\boldsymbol{\chi}_n^{k+1} = \boldsymbol{\chi}_n^k + \delta\boldsymbol{\chi}_n^k$ with $D\mathscr{R}\left(\boldsymbol{\chi}_n^k\right)\left[\delta\boldsymbol{\chi}_n^k\right] = -\mathscr{R}\left(\boldsymbol{\chi}_n^k\right)$. The initial value $\boldsymbol{\chi}_n^0$ is assigned by using a second-order extrapolation. For ease of exposition, we drop the subscript n referring to the time whenever it is clear from the context. We first provide some useful directional derivatives:

$$\begin{aligned}
&2J_s \, DJ_s\left[\delta\hat{\mathbf{B}}_\Gamma\right] = \left(\hat{\mathbf{B}}_\Gamma : \boldsymbol{\pi}_\Gamma\right)\left(\delta\hat{\mathbf{B}}_\Gamma : \boldsymbol{\pi}_\Gamma\right) - \delta\hat{\mathbf{B}}_\Gamma\boldsymbol{\pi}_\Gamma : \boldsymbol{\pi}_\Gamma\hat{\mathbf{B}}_\Gamma \\
&\quad = \left(\left(\hat{\mathbf{B}}_\Gamma : \boldsymbol{\pi}_\Gamma\right)\mathbf{I} - \hat{\mathbf{B}}_\Gamma\boldsymbol{\pi}_\Gamma\right)\delta\hat{\mathbf{B}}_\Gamma : \boldsymbol{\pi}_\Gamma; \\
&2DI_2^s\left[\delta\hat{\mathbf{B}}_\Gamma\right] = \delta\hat{\mathbf{B}}_\Gamma : \boldsymbol{\pi}_\Gamma; \\
&2J_s^3 \, DJ_s^{-1}\left[\delta\hat{\mathbf{B}}_\Gamma\right] = \left(\hat{\mathbf{B}}_\Gamma\boldsymbol{\pi}_\Gamma - \left(\hat{\mathbf{B}}_\Gamma : \boldsymbol{\pi}_\Gamma\right)\mathbf{I}\right)\delta\hat{\mathbf{B}}_\Gamma : \boldsymbol{\pi}_\Gamma; \\
&2J_s^5 \, D\left(I_2^s/J_s^3\right)\left[\delta\hat{\mathbf{B}}_\Gamma\right] = J_s^2\delta\hat{\mathbf{B}}_\Gamma : \boldsymbol{\pi}_\Gamma - 3I_2^s\left(\left(\hat{\mathbf{B}}_\Gamma : \boldsymbol{\pi}_\Gamma\right)\boldsymbol{\pi}_\Gamma - \boldsymbol{\pi}_\Gamma\hat{\mathbf{B}}_\Gamma\boldsymbol{\pi}_\Gamma\right) : \delta\hat{\mathbf{B}}_\Gamma.
\end{aligned}$$

For any $\boldsymbol{u}, \boldsymbol{v} \in H^1(\Lambda)^d$; $q \in \mathbb{Q}$; $\boldsymbol{\tau}, \boldsymbol{T} \in \mathbb{W}$; $w \in L^\infty(\Lambda)$ and $\boldsymbol{P} \in L^\infty(\Lambda)^{d\times d}$, we introduce the following multilinear forms:

$$\begin{aligned}
&a(\boldsymbol{u}, \boldsymbol{v}; w) = \int_\Lambda 2w \, \mathbf{D}(\boldsymbol{u}) : \mathbf{D}(\boldsymbol{v}); \quad b(\boldsymbol{u}, q; \boldsymbol{P}) = -\int_\Lambda q \, \boldsymbol{P} : \boldsymbol{\nabla u}; \quad c(\boldsymbol{T}, \boldsymbol{\tau}; \boldsymbol{u}) = \int_\Lambda \mathbf{sym}\left(\boldsymbol{\nabla u}\boldsymbol{T}\right) : \boldsymbol{\tau}; \\
&d(\boldsymbol{\tau}, \boldsymbol{v}; w, \boldsymbol{P}) = \int_\Lambda w\,\boldsymbol{\tau} : \left(\boldsymbol{P}\boldsymbol{\nabla v}\boldsymbol{P}\right); \quad e(\boldsymbol{T}, \boldsymbol{v}; w, \boldsymbol{P}, \boldsymbol{\tau}) = \int_\Lambda w\Big(\left((\boldsymbol{\tau} : \boldsymbol{P})\mathbf{I} - \boldsymbol{\tau}\boldsymbol{P}\right)\boldsymbol{T} : \boldsymbol{P}\Big)\left(\boldsymbol{\tau} : \boldsymbol{P}\boldsymbol{\nabla v}\boldsymbol{P}\right); \\
&f(\boldsymbol{T}, \boldsymbol{v}; \boldsymbol{P}, \boldsymbol{\tau}) = \int_\Lambda \left(\boldsymbol{\tau}\boldsymbol{T} : \boldsymbol{P}\right)\left(\boldsymbol{\nabla v} : \boldsymbol{P}\right); \quad g(\boldsymbol{T}, \boldsymbol{\tau}) = \int_\Lambda \boldsymbol{T} : \boldsymbol{\tau}; \quad m(\boldsymbol{u}, \boldsymbol{v}; w) = \int_\Lambda w\,\boldsymbol{u} \cdot \boldsymbol{v}.
\end{aligned}$$

Therefore, the exact tangent problem associated to the correction step reads: find $\delta\boldsymbol{\chi}^k \in \mathbb{V}(\boldsymbol{u}_b) \times \mathbb{Q} \times \mathbb{W}$ such that

$$\begin{aligned}
&\frac{3}{2\Delta t} m\Big(\delta\boldsymbol{u}^k, \boldsymbol{v}; \rho_\varepsilon(\varphi_n)\Big) + a\Big(\delta\boldsymbol{u}^k, \boldsymbol{v}; \mu_\varepsilon(\varphi_n)\Big) + b\Big(\boldsymbol{v}, \delta p^k; \mathbf{I}\Big) \\
&\qquad + \frac{E_s}{3} d\left(\delta\hat{\mathbf{B}}_\Gamma^k, \boldsymbol{v}; \left(\frac{\zeta}{(J_s^k)^3} + \frac{1-\zeta}{J_s^k}\right) |\boldsymbol{\nabla}\varphi_n| \delta_\varepsilon(\varphi_n), \boldsymbol{\pi}_{\Gamma,n}\right) \\
&\qquad + \frac{E_s}{3} f\left(\delta\hat{\mathbf{B}}_\Gamma^k, \boldsymbol{v}; \boldsymbol{\pi}_{\Gamma,n}, \left(\frac{\zeta\big((J_s^k)^4 + 6I_2^s + 3\big) + 3}{2(J_s^k)^5}\Big((\hat{\mathbf{B}}_\Gamma^k : \boldsymbol{\pi}_{\Gamma,n})\mathbf{I} - \hat{\mathbf{B}}_\Gamma^k \boldsymbol{\pi}_{\Gamma,n}\Big)\right.\right. \\
&\qquad \left.\left. - \frac{\zeta}{2(J_s^k)^3}\mathbf{I}\right) |\boldsymbol{\nabla}\varphi_n| \delta_\varepsilon(\varphi_n)\right) \\
&\qquad - \frac{E_s}{3} e\left(\delta\hat{\mathbf{B}}_\Gamma^k, \boldsymbol{v}; \left(\frac{3\zeta}{2(J_s^k)^5} + \frac{1-\zeta}{2(J_s^k)^3}\right) |\boldsymbol{\nabla}\varphi_n| \delta_\varepsilon(\varphi_n), \boldsymbol{\pi}_{\Gamma,n}, \hat{\mathbf{B}}_\Gamma^k\right) \\
&\qquad = -\Big\langle \mathscr{R}_{\boldsymbol{\chi}}\left(\boldsymbol{\chi}^k\right), \boldsymbol{v}\Big\rangle_{\mathbb{V}(\mathbf{0})', \mathbb{V}(\mathbf{0})}, \\
&b\Big(\delta\boldsymbol{u}^k, q; \mathbf{I}\Big) = -\Big\langle \mathscr{R}_p\left(\boldsymbol{u}^k\right), q\Big\rangle_{\mathbb{Q}', \mathbb{Q}}, \\
&\frac{3}{2\Delta t} g\left(\delta\hat{\mathbf{B}}_\Gamma^k, \boldsymbol{\tau}\right) - c\left(\delta\hat{\mathbf{B}}_\Gamma^k, \boldsymbol{\tau}; \boldsymbol{u}^k\right) - c\left(\hat{\mathbf{B}}_\Gamma^k, \boldsymbol{\tau}; \delta\boldsymbol{u}^k\right) = -\Big\langle \mathscr{R}_{\boldsymbol{u}, \hat{\mathbf{B}}_\Gamma}(\boldsymbol{u}^k, \hat{\mathbf{B}}_\Gamma^k), \boldsymbol{\tau}\Big\rangle_{\mathbb{W}', \mathbb{W}},
\end{aligned}$$

for all $\boldsymbol{v} \in \mathbb{V}(\mathbf{0})$, $q \in \mathbb{Q}$ and $\boldsymbol{\tau} \in \mathbb{W}$. The corresponding residuals are expressed as:

$$\begin{aligned}
\Big\langle \mathscr{R}_{\boldsymbol{\chi}}\left(\boldsymbol{\chi}^k\right), \boldsymbol{v}\Big\rangle &= \frac{1}{2\Delta t} m\Big(3\boldsymbol{u}^k - 4\boldsymbol{u}_{n-1} + \boldsymbol{u}_{n-2}, \boldsymbol{v}; \rho_\varepsilon(\varphi_n)\Big) + a\Big(\boldsymbol{u}^k, \boldsymbol{v}; \mu_\varepsilon(\varphi_n)\Big) + b\Big(\boldsymbol{v}, p^k; \mathbf{I}\Big) \\
&\quad + \frac{E_s}{3} d\left(\hat{\mathbf{B}}_\Gamma^k, \boldsymbol{v}; \left(\frac{\zeta}{(J_s^k)^3} + \frac{1-\zeta}{J_s^k}\right) |\boldsymbol{\nabla}\varphi_n| \delta_\varepsilon(\varphi_n), \boldsymbol{\pi}_{\Gamma,n}\right) \\
&\quad - \frac{E_s}{3} b\left(\boldsymbol{v}, \left(\zeta J_s^k - 2\zeta \frac{(I_2^s)^k}{(J_s^k)^3} - \frac{1+\zeta}{(J_s^k)^3}\right) |\boldsymbol{\nabla}\varphi_n| \delta_\varepsilon(\varphi_n); \boldsymbol{\pi}_{\Gamma,n}\right), \\
\Big\langle \mathscr{R}_p\left(\boldsymbol{u}^k\right), q\Big\rangle &= b\Big(\boldsymbol{u}^k, q; \mathbf{I}\Big) \quad \text{and} \\
\Big\langle \mathscr{R}_{\boldsymbol{u}, \hat{\mathbf{B}}_\Gamma}\left(\boldsymbol{u}^k, \hat{\mathbf{B}}_\Gamma^k\right), \boldsymbol{\tau}\Big\rangle &= c\Big(\hat{\mathbf{B}}_\Gamma^k, \boldsymbol{\tau}; \boldsymbol{u}^k\Big) + \frac{1}{2\Delta t} g\Big(3\hat{\mathbf{B}}_\Gamma^k - 4\hat{\boldsymbol{B}}_{\Gamma,n-1} + \hat{\boldsymbol{B}}_{\Gamma,n-2}, \boldsymbol{\tau}\Big).
\end{aligned}$$

4. Sample numerical results

This framework has been implemented using the Rheolef environment for scientific computing [11]. Parallelism relies on MPI,[1] while MUMPS[2] is used for the factorization and as direct solver on distributed-memory architectures.

First, consider the test case described in [12]. The domain spans the region $[0,1.5]^2$ and we model the relaxation of a stretched ellipsoidal membrane initially having the semi-major and semi-minor axes $a = 0.75$ and $b = 0.5$ and centered at (0.75,0.75). The membrane stretching is initially $\mathsf{J}_s(0) \approx 1.2625316$. The mechanics is restricted to the stretching [12] and we consider a linear stress–strain relationship $\mathsf{W}'(J_s) = E_s(J_s - 1)$ where $E_s = 2.7$ is the membrane tension coefficient. We set $\rho_{i/o} = 1$ and $\mu_{i/o} = 0.015$ and prescribe the no-slip wall condition ($\boldsymbol{u}_b = \mathbf{0}$). Under the effect of the elastic force, the stretched ellipse starts oscillating toward an equilibrium circular and stretched steady state having the radius $\sqrt{ab}$ (enclosed area preserved), in which the membrane force vanishes. See snapshots in Fig. 2.

[1] Message Passing Interface—http://www.mpi-forum.org.
[2] MUMPS package—http://graal.ens-lyon.fr/MUMPS.

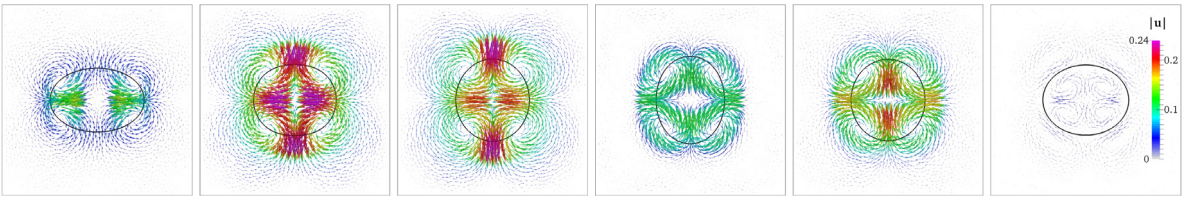

Fig. 2. Snapshots showing $\Gamma(t)$ (black contour) and $\boldsymbol{u}$ at successive times during the first relaxation period $t \in \{0.12, 0.56, 0.9, 1.68, 2, 2.8\}$.

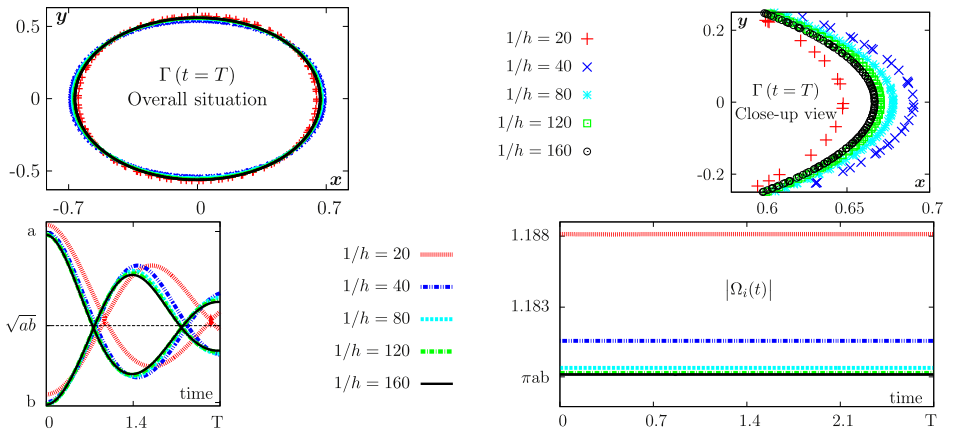

Fig. 3. Comparison of final shapes and temporal evolution of the axes and $|\Omega_i|$ for different spatial resolutions. The same colorbar is used. (For interpretation of the references to color in this figure legend, the reader is referred to the web version of this article.)

	$1/h$	$\|e\|_1$	ROC	$\|e\|_2$	ROC	$\|e\|_\infty$	ROC
$a(t)$	20	2.635E−2		2.657E−2		2.953E−2	
	40	7.758E−3	2.917	7.899E−3	1.750	9.313E−3	1.665
	80	1.149E−3	2.755	9.913E−4	2.994	1.517E−3	2.618
	120	3.320E−4	3.062	2.847E−4	3.077	4.617E−4	2.933
$\phi(t)$	20	2.561E−3	4.152	2.925E−3	4.083	4.465E−3	3.833
	40	5.189E−4	2.303	5.712E−4	2.357	9.443E−4	2.241
	80	1.267E−4	2.034	1.499E−4	1.930	3.098E−4	1.608
	120	5.046E−5	2.271	6.525E−5	2.051	1.658E−4	1.542

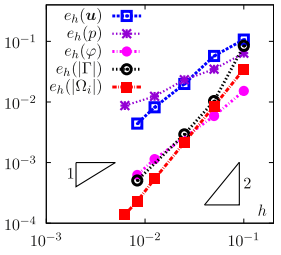

Fig. 4. Convergence history with respect to the spatial resolution and experimental orders of convergence for a, ϕ, $|\Omega_i|$, $|\Gamma|$, $\boldsymbol{u}$, p and φ.

To study with the spatial convergence of the proposed numerical scheme, we consider the time horizon $(0, T = 2.8)$ and a family of unstructured meshes. Let $\phi(t) = 2\sqrt{\pi|\Omega_i|}/|\Gamma|$ be the degree of circularity. In the absence of analytical solutions, we proceed with quantitative comparisons with a reference solution obtained using the finer mesh and smaller Δt. In Fig. 3, comparisons of the shapes at time T, the detailed view in the zone of maximal discrepancy and the temporal evolution of the membrane axes reveal quit good congruence for finer resolutions. Results depict a good mass preservation. Following [8], the spatial accuracy of the approximation of a quantity ξ_t is measured by computing normalized errors on successively refined meshes against a reference solution ξ_t^r (with $h = 1/160$). We compute:

$$|e|_1 = \frac{\sum_{t=1}^{N}|\xi_t^r - \xi_t|}{\sum_{t=1}^{N}|\xi_t^r|}, \qquad |e|_2^2 = \frac{\sum_{t=1}^{N}|\xi_t^r - \xi_t|^2}{\sum_{t=1}^{N}|\xi_t^r|^2}, \qquad |e|_\infty = \frac{\max_t|\xi_t^r - \xi_t|}{\max_t|\xi_t^r|}$$

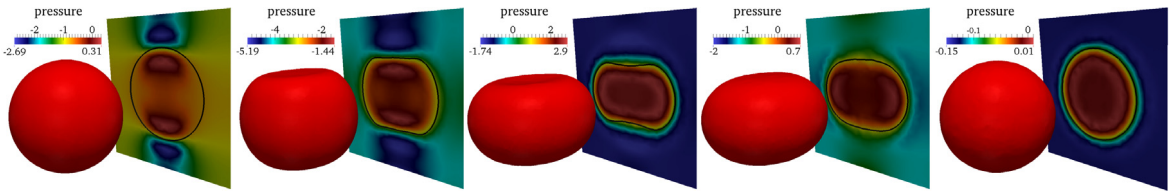

Fig. 5. Snapshots showing the relaxation of the membrane Γ in three dimensions at successive times $t \in \{0.02, 0.4, 1.24, 1.4, 9.3\}$, respectively.

and the convergence rate

$$\text{ROC} = \frac{\ln\left(|e^{l-1}|/|e^{l}|\right)}{\ln\left(h^{l-1}/h^{l}\right)} \qquad \text{where l is the mesh refinement level.}$$

Results in Fig. 4 (left) suggest that the semi-major axis a approaches a convergence order of 3 in all norms. The circularity approaches a convergence order of 2 in the l_1 and l_2 norms, while it decreases to 1.5 in the l_∞ norm. To study the relative spatial errors of a given field ξ with respect to the reference solution, we compute $e_h(\xi) = \|\xi_h(.,T) - \xi_h^r(.,T)\|_{0,\Omega} / \|\xi_h^r(.,T)\|_{0,\Omega}$. Results in Fig. 4 (right) suggest that the convergence rates for $\boldsymbol{u}$ and p are suboptimal. That is mainly due to the regularization procedure and the inability of the approximation spaces to capture the stress discontinuities across Γ. As a remedy to retrieve the optimal rates, one can locally adapt the mesh to capture the membrane position and incorporate the correct stress jump [2] but this is beyond the scope of this work.

As a three-dimensional test case, the membrane elasticity is described using the Mooney–Rivlin model. Consider an unstressed sphere of radius 0.4 centered in a computational domain $[-1,1]^3$. We set the parameters: $\zeta = 0.5$, $E_s = 15$, $\rho_{i/o} = 1$ and $\mu_{i/o} = 0.35$. Initially, both fluids are at rest and homogeneous Dirichlet boundary conditions $\boldsymbol{u}_b = \boldsymbol{0}$ are considered. For $t \in [0.1]$, a compression vertical force in opposite directions is applied to the membrane:

$$\boldsymbol{F}_{\text{ext}} = 5\mathscr{H}_\varepsilon\left(x^2 + y^2 - 0.3\right)\left(2\mathscr{H}_\varepsilon(z) - 1\right)\delta_\varepsilon(\varphi)\boldsymbol{z} \qquad \text{at } (x,y,z) \in \Lambda.$$

The membrane is relaxed at time $t = 1$, resulting in the gradual decrease of the membrane elastic force which vanishes when the unstressed spherical shape is recovered. Snapshots in Fig. 5 show the shapes of the membrane during the compression and relaxation phases. Remark that the increase in the pressure jump across Γ compensates the increase of the membrane stress during the compression phase. The quadratic convergence of the Newton algorithm is clearly observed in Fig. 6 (a–b). For large Δt or E_s, we first observe a slow convergence until the residual reaches a threshold value, beyond it the quadratic convergence is achieved.

We now proceed with comparison with a partitioned strongly-coupled strategy that consists in iterating at each time step between the subproblems (2.1), (2.3)–(2.4) and (2.2) until reaching the convergence (fixed-point loop). We report in Fig. 6 (right) the computing times. When increasing the elastic modulus the present method performs significantly better than the partitioned approach which features a very slow convergence of the fixed-point sub-iterations.

5. Conclusion

A predictor–corrector method based on operator splitting and Newton algorithms has been developed to model elastic membranes in an incompressible flow. It features an affordable computational burden compared to the fully implicit methods for which the computing times could be prohibitive. The application of the

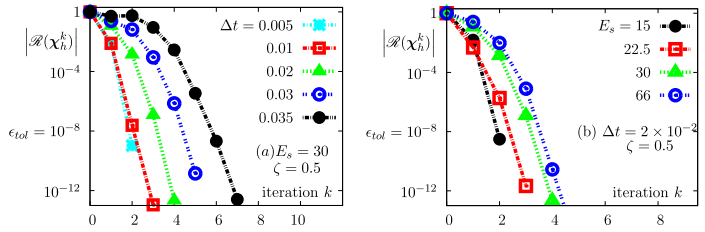

	Solution time	
	Present method	Fully implicit strategy
$E_s = 0.75$	1h 31min 59s	1h 8min 41s
$E_s = 3$	1h 56min 40s	2h 0min 51s
$E_s = 30$	5h 12min 12s	10h 54min 35s

(c)

Fig. 6. Convergence of the Newton algorithm: residuals' curves versus the iteration number for several (a) Δt and (b) E_s. (c) Comparison of the timings with respect to the partitioned fully implicit strategy for the simulation period $(0, T = 1)$ using $\rho_{i/o} = 1$, $\mu_{i/o} = 0.1$ and $94'617$ degrees of freedom. Parallel simulations were performed using five cores on a computing platform with Intel® Core™ i7-4790 (3.6 GHz) processors.

method is more general for a wide range of FSI and capillarity problems and not only relevant to RBCs. This is part of an ongoing work to model RBCs and we foresee the coupling with the highly nonlinear bending force [1,7,13]. Improvements to accurately capture the solution discontinuities across the membrane are currently being explored [14].

References

[1] R. Skalak, A. Tozeren, R. Zarda, S. Chien, Strain energy function of red blood cell membranes, Biophys. J. 13 (3) (1973) 245–264.
[2] S. Xu, Z.J. Wang, An immersed interface method for simulating the interaction of a fluid with moving boundaries, J. Comput. Phys. 216 (2) (2006) 454–493.
[3] H. Wei-Fan, K. Yongsam, M.-C. Lai, An immersed boundary method for simulating the dynamics of three-dimensional axisymmetric vesicles in Navier-Stokes flows, J. Comput. Phys. 257 (2014) 670–686, Part A.
[4] G.-H. Cottet, E. Maitre, A level-set formulation of immersed boundary methods for fluid-structure interaction problems, C. R. Math. 338 (7) (2004) 581–586.
[5] B. Griffith, On the volume conservation of the immersed boundary method, Commun. Comput. Phys. 12 (2012) 401–432.
[6] D. Barthès-Biesel, J. Rallison, The time-dependent deformation of a capsule freely suspended in a linear shear flow, J. Fluid Mech. 113 (1981) 251–267.
[7] A. Laadhari, P. Saramito, C. Misbah, G. Székely, Fully implicit methodology for the dynamics of biomembranes and capillary interfaces by combining the level set and newton methods, J. Comput. Phys. 343 (2017) 271–299.
[8] A. Laadhari, Exact Newton method with third-order convergence to model the dynamics of bubbles in incompressible flow, Appl. Math. Lett. 69 (2017) 138–145.
[9] A. Caboussat, A numerical method for the simulation of free surface flows with surface tension, Comput. & Fluids 35 (10) (2006) 1205–1216.
[10] J. Kou, Y. Li, X. Wang, A modification of Newton method with third-order convergence, Appl. Math. Comput. 181 (2) (2006) 1106–1111.
[11] Efficient C++ finite element computing with Rheolef, https://www-ljk.imag.fr/membres/Pierre.Saramito/rheolef/ (Accessed: 01.01.18).
[12] Z. Tan, D. Le, Z. Li, K. Lim, B. Khoo, An immersed interface method for solving incompressible viscous flows with piecewise constant viscosity across a moving elastic membrane, J. Comput. Phys. 227 (23) (2008) 9955–9983.
[13] M.-C. Lai, Y. Seol, A short note on Navier-Stokes flows with an incompressible interface and its approximations, Appl. Math. Lett. 65 (2017) 1–6.
[14] E.M. Kolahdouz, D. Salac, A numerical model for the trans-membrane voltage of vesicles, Appl. Math. Lett. 39 (2015) 7–12.